



# CHORUS

This is the accepted manuscript made available via CHORUS. The article has been published as:

## Tunable electronic anisotropy in single-crystal $A_{2}Cr_{3}As_{3}$ ( $A=K, Rb$ ) quasi-one-dimensional superconductors

X. F. Wang, C. Roncaioli, C. Eckberg, H. Kim, J. Yong, Y. Nakajima, S. R. Saha, P. Y. Zavalij, and J. Paglione

Phys. Rev. B **92**, 020508 — Published 20 July 2015

DOI: [10.1103/PhysRevB.92.020508](https://doi.org/10.1103/PhysRevB.92.020508)

# Tunable electronic anisotropy in single-crystal $A_2Cr_3As_3$ ( $A = K, Rb$ ) quasi-one-dimensional superconductors

X. F. Wang,<sup>1</sup> C. Roncaioli,<sup>1</sup> C. Eckberg,<sup>1</sup> H. Kim,<sup>1</sup> J. Yong,<sup>1</sup>  
Y. Nakajima,<sup>1</sup> S. R. Saha,<sup>1</sup> P.Y. Zavalij,<sup>2</sup> and J. Paglione<sup>1,3</sup>

<sup>1</sup>Center for Nanophysics and Advanced Materials,

Department of Physics, University of Maryland, College Park, MD 20742

<sup>2</sup>Department of Chemistry, University of Maryland, College Park, Maryland 20742, USA

<sup>3</sup>Canadian Institute for Advanced Research, Toronto, Canada M5G 1Z8

(Dated: June 26, 2015)

Single crystals of  $A_2Cr_3As_3$  ( $A = K, Rb$ ) were successfully grown using a self-flux method and studied via structural, transport and thermodynamic measurement techniques. The superconducting state properties between the two species are similar, with critical temperatures of 6.1 K and 4.8 K in  $K_2Cr_3As_3$  and  $Rb_2Cr_3As_3$ , respectively. However, the emergence of a strong normal state electronic anisotropy in  $Rb_2Cr_3As_3$  suggests a unique electronic tuning parameter is coupled to the inter-chain spacing in the  $A_2Cr_3As_3$  structure, which increases with alkali metal ionic size while the one-dimensional  $[(Cr_3As_3)^{2-}]_{\infty}$  chain structure itself remains essentially unchanged. Together with dramatic enhancements in both conductivity and magnetoresistance (MR), the appearance of a strong anisotropy in the MR of  $Rb_2Cr_3As_3$  is consistent with the proposed quasi-one-dimensional character of band structure and its evolution with alkali metal species in this new family of superconductors.

PACS numbers: 74.25.-q, 74.25.Ha, 75.30.-m

The recent discovery of superconductivity in  $A_2Cr_3As_3$  ( $A = K$  [1],  $Rb$  [2] and  $Cs$  [3]) has garnered significant attention due to the possible presence of reduced dimensionality in both normal and superconducting state properties. Superconductivity in quasi-one-dimensional (quasi-1D) systems presents a unique set of properties, including exotic deviations from expected behavior such as found in orbital magnetic field properties, as well as unconventional pairing in the form of singlet  $d$ -wave [4] and triplet  $p$ -wave [5] order parameters that emerge.

The crystal structure of  $A_2Cr_3As_3$  indeed has one-dimensional elements, composed of double-walled subnanotube  $[Cr_3As_3]_{\infty}$  chains separated by alkali metal atoms in a hexagonal unit cell, as shown in Fig. 1. This chain crystal structure is quite similar to the well known quasi-1D superconductors such as the Bechgaard salts [6, 7], and purple bronzes  $Li_{0.9}Mo_6O_{17}$  [8] and  $Tl_2Mo_6Se_6$  [9]. The reported superconducting state properties show some indications of reduced dimensions, including a very large upper critical field  $H_{c2}$  that exceeds the Pauli limit [1, 2, 10], and provide some evidence for an unconventional pairing mechanism, as evidenced by power law behavior in specific heat [2] and penetration depth measurements [11] on polycrystalline samples, as well as strong magnetic fluctuations in nuclear magnetic resonance [12] measurements. However, due to the difficulties in interpreting measured properties of polycrystalline samples with potential low-dimensional aspects, it is imperative that single-crystalline samples are studied. For instance, reports of an unusual linear temperature dependence of resistivity in polycrystalline samples of  $K_2Cr_3As_3$  and  $Rb_2Cr_3As_3$  [1, 2] have been contradicted by a recent single-crystal study of  $K_2Cr_3As_3$  [10], which

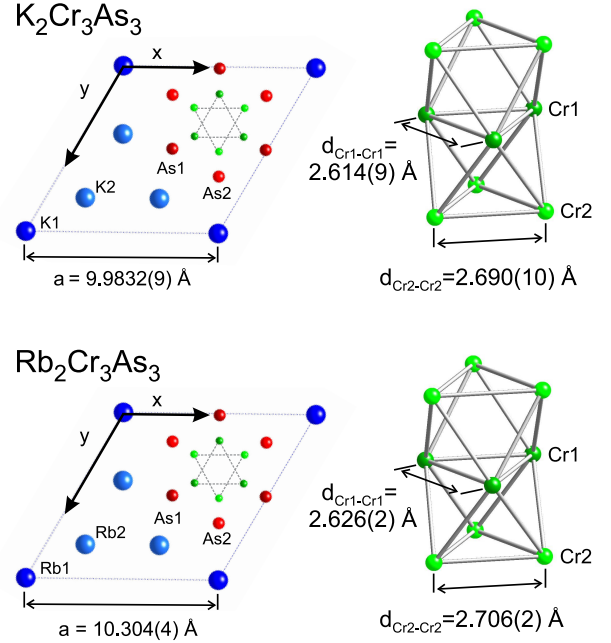


FIG. 1: Schematic view of structure of  $K_2Cr_3As_3$  and  $Rb_2Cr_3As_3$ . The detail comparison of the lattice parameters are listed in Table II. Data for  $K_2Cr_3As_3$  is from Ref. 1.

also reports a relatively weak anisotropy of the amplitude of  $H_{c2}$  between fields applied parallel ( $H_{\parallel}$ ) and perpendicular ( $H_{\perp}$ ) to the needle-like crystal orientation, which is the  $(00l)$  direction of the crystal structure, raising the question about the dimensionality of the electronic structure in the  $A_2Cr_3As_3$  family.

Here we report the successful growth of both  $\text{K}_2\text{Cr}_3\text{As}_3$  and  $\text{Rb}_2\text{Cr}_3\text{As}_3$  single crystals and their normal and superconducting state properties based on structural, transport, magnetic and thermodynamic measurements. Comparing normal state transport properties between  $\text{K}_2\text{Cr}_3\text{As}_3$  and  $\text{Rb}_2\text{Cr}_3\text{As}_3$  single crystal samples reveals several key differences, including a large increase in the electrical conductivity in  $\text{Rb}_2\text{Cr}_3\text{As}_3$  consistent with the proposed band structure evolution, as well as the emergence of a strong magnetoresistance magnitude and anisotropy in  $\text{Rb}_2\text{Cr}_3\text{As}_3$  that we relate to a tunable reduced structural dimensionality that is controlled by the alkali metal species in the  $\text{A}_2\text{Cr}_3\text{As}_3$  system.

$\text{K}_2\text{Cr}_3\text{As}_3$  and  $\text{Rb}_2\text{Cr}_3\text{As}_3$  single crystals were grown using a self-flux method as previously reported [1, 10]. Pieces of K and Rb alkali metal (99.8%, Alfa Aesar) and chromium (99.999%, Alfa Aesar) were combined with arsenic powder (99.99%, Alfa Aesar) into an alumina crucible and sealed in a nitrogen glove box using a stainless steel tube/swagelok cap configuration [13]. Growths were heated up to 1000 °C and kept at this temperature for one day, followed by slow cooling down to 650 °C. The swagelok enclosure was then re-opened in a glovebox, revealing many single crystals with shiny, silver coloring and a thin, long needle-like shape that extends along the crystallographic [001] axis. Crystals were mechanically removed from the crucibles and visually inspected for residual flux and crystalline quality. We note that  $\text{Rb}_2\text{Cr}_3\text{As}_3$  crystals are much more reactive than  $\text{K}_2\text{Cr}_3\text{As}_3$ , resulting in larger uncertainties in sample mass determinations. Resistivity measurements were performed using the standard four-terminal configuration in a commercial cryostat system. Contacts were made in a glovebox using silver paint, followed by coating of samples with Apiezon N-grease to avoid air exposure. Magnetization measurement were taken using both a commercial SQUID magnetometer and vibrating sample magnetometer for  $\text{K}_2\text{Cr}_3\text{As}_3$  and  $\text{Rb}_2\text{Cr}_3\text{As}_3$  samples, respectively. A needle-like specimen of  $\text{Rb}_2\text{Cr}_3\text{As}_3$  with approximate dimensions 0.01 mm  $\times$  0.03 mm  $\times$  0.39 mm was used for x-ray crystallographic analysis with intensity data measured using a Bruker APEX-II CCD system equipped with a graphite monochromator and a MoK $\alpha$  sealed tube ( $\lambda = 0.71073$  Å), with data collection performed at 90 K and 250 K. The structure was solved and refined using the Bruker SHELXTL Software Package, using the space group  $\text{P}\bar{6}\text{m}2$ , with  $Z = 2$  for the formula unit,  $\text{Rb}_2\text{Cr}_3\text{As}_3$ . The final anisotropic full-matrix least-squares refinement on  $F^2$  with 23 variables converged to  $R1$  ( $wR2$ ) = 3.39% (8.37%) and 3.85% (9.96%) at 90 K and 250 K, respectively.

The lattice parameters of  $\text{Rb}_2\text{Cr}_3\text{As}_3$  are larger than those of  $\text{K}_2\text{Cr}_3\text{As}_3$ , with the larger ionic radius of Rb (1.52 Å) as compared to K (1.38 Å) increasing the spacing between the  $[\text{Cr}_3\text{As}_3]_\infty$  chains as shown in Fig. 1. Table I presents the atomic coordinates obtained from

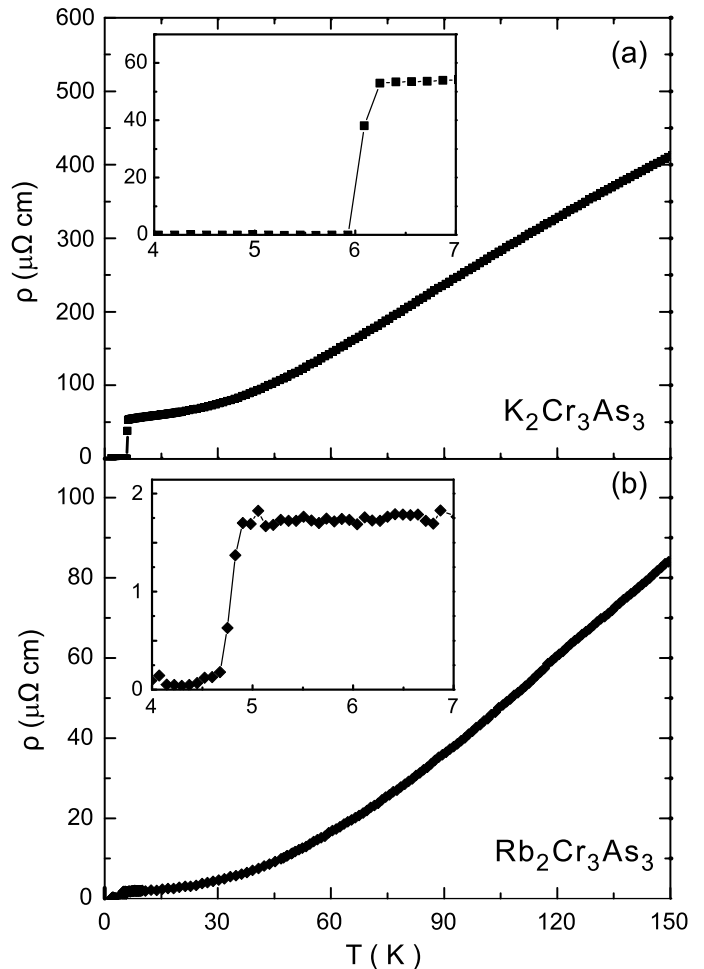


FIG. 2: Resistivity of  $\text{K}_2\text{Cr}_3\text{As}_3$  and  $\text{Rb}_2\text{Cr}_3\text{As}_3$  single crystals measured along the [001] crystallographic (needle) direction, shown in panels (a) and (b), respectively. Insets present low-temperature zoom, highlighting the superconducting transition in each compound.

TABLE I: Atomic coordinates for  $\text{Rb}_2\text{Cr}_3\text{As}_3$  single crystal, measured at 250 K.

Atom	Label	x	y	z	Wyckoff position	$U_{eq}$
Rb	Rb1	0.0	0.0	0.0	3j	0.0279(10)
Rb	Rb2	0.79519(14)	0.5904(3)	0.5	3k	0.0232(5)
Cr	Cr1	0.4183(2)	0.8366(4)	0.5	3k	0.0115(7)
Cr	Cr2	0.5084(5)	0.7542(2)	0.0	3j	0.0122(7)
As	As1	0.49505(14)	0.9901(3)	0.0	1c	0.0125(5)
As	As2	0.6581(3)	0.82907(15)	0.5	3k	0.0124(5)

single-crystal x-ray analysis of  $\text{Rb}_2\text{Cr}_3\text{As}_3$ , with results well refined using a hexagonal crystal structure ( $\text{P}\bar{6}\text{m}2$ ) and showing no symmetry changes when cooling down to 90 K. The unit cell of  $\text{Rb}_2\text{Cr}_3\text{As}_3$  is 3.2% and 0.5% larger than that of  $\text{K}_2\text{Cr}_3\text{As}_3$  [1] along the  $a$ - and  $c$ -axis directions, respectively. However, in contrast to the chain structure distortion previously reported for polycrystalline samples [1], the  $[(\text{Cr}_3\text{As}_3)^{2-}]_\infty$  chain trunk

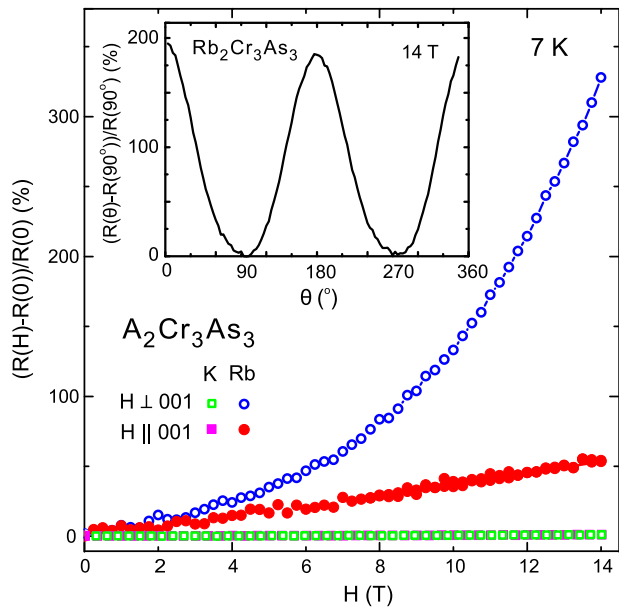


FIG. 3: Normalized magnetoresistance of  $\text{K}_2\text{Cr}_3\text{As}_3$  and  $\text{Rb}_2\text{Cr}_3\text{As}_3$  single crystal samples measured at 7 K under different field orientation configurations, with current applied along the needle ([001]) direction. The inset presents the field angle-dependent resistivity of  $\text{Rb}_2\text{Cr}_3\text{As}_3$  at 7 K and 14 T.

width is almost identical for  $\text{Rb}_2\text{Cr}_3\text{As}_3$  and  $\text{K}_2\text{Cr}_3\text{As}_3$  as shown in Table II, displayed more clearly in Fig. 1. The Cr1-Cr1, Cr1-Cr2 and Cr2-Cr2 bond distances change less than 0.6% between  $\text{K}_2\text{Cr}_3\text{As}_3$  and  $\text{Rb}_2\text{Cr}_3\text{As}_3$ , while the alkali metal-arsenic bonds change by 3-4%, consistent with a more simple expansion of the interchain distances with larger alkali metal units and almost no influence on the chain structure itself. This presents a unique ability to tune the electronic density of a system while keeping the important structural elements unchanged, providing for an interesting “knob” to use for studying the emergence of reduced dimensional properties.

The electrical resistivity of  $\text{K}_2\text{Cr}_3\text{As}_3$  and  $\text{Rb}_2\text{Cr}_3\text{As}_3$  single crystals along the [001] needle direction is presented in Fig. 2, showing  $T_c$  values of 6.1 K and 4.8 K, respectively, consistent with previous reports [1, 2, 10]. Transport behavior of  $\text{K}_2\text{Cr}_3\text{As}_3$  crystals is quite similar to that previously reported for single-crystal samples [10], showing a marked difference in the temperature dependence as compared to polycrystalline samples that exhibit an anomalous linear temperature dependence above  $T_c$  [1-3]. The residual resistivity ratio  $RRR=R(300\text{ K})/R(7\text{ K})$  for  $\text{K}_2\text{Cr}_3\text{As}_3$  is 15, slightly larger than the reported value of 10 for polycrystals [1, 10] and smaller than in previous work [10]. For the latter study, the reported ratio is 50 while the residual resistivity of  $\rho_0 \simeq 25\ \mu\Omega\text{cm}$  is about half of the value measured in this study, indicating a notable sample dependence of resistivity without a notable change in  $T_c$ . For single-crystal  $\text{Rb}_2\text{Cr}_3\text{As}_3$  synthesized in the exact same

TABLE II: Comparison of crystallographic data for  $\text{K}_2\text{Cr}_3\text{As}_3$  (300 K) [1] and  $\text{Rb}_2\text{Cr}_3\text{As}_3$  (250 K and 90 K).

	$\text{K}_2\text{Cr}_3\text{As}_3$ [1] 300 K	$\text{Rb}_2\text{Cr}_3\text{As}_3$ 250 K	$\text{Rb}_2\text{Cr}_3\text{As}_3$ 90 K
space group	$\text{P}\bar{6}\text{m}2$	$\text{P}\bar{6}\text{m}2$	$\text{P}\bar{6}\text{m}2$
a(Å)	9.9832(9)	10.304(4)	10.251(5)
c(Å)	4.2304(4)	4.2514(18)	4.227(2)
V(Å <sup>3</sup> )	365.13(6)	390.9(4)	384.7(4)
<b>Bond distance (A=K and Rb)</b>			
A1-As1(Å)	3.366(2)	3.484(2)	3.462(2)
A1-As2(Å)	3.263(5)	3.393(2)	3.375(2)
A2-As1(Å)	4.9916(13)	5.153(2)	5.126(2)
A2-As2(Å)	3.562(3)	3.718(2)	3.693(2)
Cr1-As1(Å)	2.516(4)	2.529(2)	2.516(2)
Cr1-As2(Å)	2.510(3)	2.511(2)	2.504(2)
Cr2-As1(Å)	2.490(3)	2.502(2)	2.494(2)
Cr2-As2(Å)	2.506(4)	2.511(2)	2.497(2)
Cr1-Cr1(Å)	2.614(9)	2.626(2)	2.616(2)
Cr1-Cr2(Å)	2.6116(15)	2.625(2)	2.613(2)
Cr2-Cr2(Å)	2.690(10)	2.706(2)	2.703(2)

manner as  $\text{K}_2\text{Cr}_3\text{As}_3$ , we obtain a much larger RRR value of 125 as compared to  $\text{K}_2\text{Cr}_3\text{As}_3$  [1, 10] and  $\text{Rb}_2\text{Cr}_3\text{As}_3$  [2] studies, likely indicating very high crystalline purity in this system and a possible sensitivity to grain boundary effects as encountered in polycrystalline studies.

Interestingly, the resistivity ( $\sim 200\ \mu\Omega\text{cm}$ ) of single-crystal  $\text{Rb}_2\text{Cr}_3\text{As}_3$  at 300 K is notably reduced compared to that of  $\text{K}_2\text{Cr}_3\text{As}_3$ , by a factor of approximately four. Assuming the phonon scattering is similar in the two compounds, this decrease may be a result of qualitative changes in the electronic structure, consistent with the theoretical prediction of significant changes in the Fermi surface by J. Wu *et al* [14], who point out that an extra quasi-1D surface near  $[0\ 0\ \pi]$  and changes in the three-dimensional surfaces could result in an increase in conductivity in  $\text{Rb}_2\text{Cr}_3\text{As}_3$  as compared to  $\text{K}_2\text{Cr}_3\text{As}_3$ . We also observe striking contrasts in the magnetoresistance (MR) of  $\text{K}_2\text{Cr}_3\text{As}_3$  and  $\text{Rb}_2\text{Cr}_3\text{As}_3$  crystals. The extremely small MR measured in  $\text{K}_2\text{Cr}_3\text{As}_3$  ( $<1\%$  at 7 K and 14 T) is similar to that found in previous work [10], with no measurable difference between the MR measured in both transverse ( $H_\perp[001]$ ) and longitudinal  $H_\parallel[001]$  configurations up to 14 T. This is in stark contrast to the MR of  $\text{Rb}_2\text{Cr}_3\text{As}_3$  (Fig. 3), which exhibits a 325% increase in  $H_\perp[001]$  MR at 7 K and 14 T that is quasi-parabolic and linear for  $H_\perp$  and  $H_\parallel$  orientations, respectively. Moreover, the anisotropy exhibits a two-fold symmetry in field-angle rotation measurements shown in Fig. 3, with a 200% change in magnitude between  $H_\perp$  and  $H_\parallel$  orientations. Considering the similarity of the two systems in all other known properties, this dramatic increase in MR and appearance of strong anisotropy is considered strong evidence for the appearance of quasi-1D components in the electronic structure, consistent with

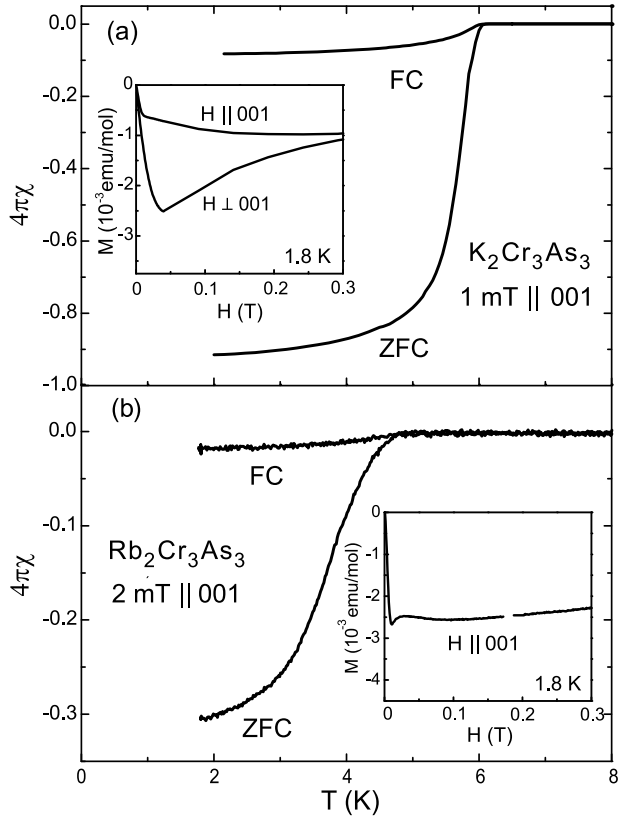


FIG. 4: Magnetic susceptibility of  $\text{K}_2\text{Cr}_3\text{As}_3$  and  $\text{Rb}_2\text{Cr}_3\text{As}_3$  single crystal collections under zero-field cooled and field-cooled conditions. Panel (a) presents measurements of  $\text{K}_2\text{Cr}_3\text{As}_3$  single crystals with 1 mT field applied along the [001] needle direction. The insert shows field dependent magnetization of  $\text{K}_2\text{Cr}_3\text{As}_3$  single crystals with field applied both parallel and perpendicular to [001]. Panel (c) presents measurements of  $\text{Rb}_2\text{Cr}_3\text{As}_3$  single crystals with 2 mT field applied along the [001] needle direction. The insert shows the field dependent magnetization for parallel ( $H_{\parallel}$ ) fields.

theoretical predictions as noted above [14].

The magnetic susceptibility  $\chi$  of  $\text{K}_2\text{Cr}_3\text{As}_3$  and  $\text{Rb}_2\text{Cr}_3\text{As}_3$  single crystals, shown in Fig. 4, confirms the onset of diamagnetic Meissner screening at the same  $T_c$  values reported above. In  $\text{K}_2\text{Cr}_3\text{As}_3$ , a shielding fraction of  $\sim 90\%$  is estimated using the zero-field-cooled  $\chi(T)$  curve, indicating a significant bulk fraction of superconductivity. In  $\text{Rb}_2\text{Cr}_3\text{As}_3$ , a smaller apparent fraction of  $\sim 30\%$  may be due to difficulties in measuring the much smaller crystals, with needle diameters of  $30 \mu\text{m}$  as compared to  $80 \mu\text{m}$  for  $\text{K}_2\text{Cr}_3\text{As}_3$  crystals, and/or due to greater errors in mass determination because of the much more reactive nature of the compound. The isothermal magnetization  $M$  was measured for both systems at 1.8 K, as shown in the insets of Fig. 4. The low-field behavior exhibits the characteristic curve of type II superconductors, where  $H_{c1}$  can be obtained from the deviation point of the linear field dependence of the  $M(H)$  curve, yielding ( $H \parallel [001]$ ) values of 90 Oe and 60 Oe in

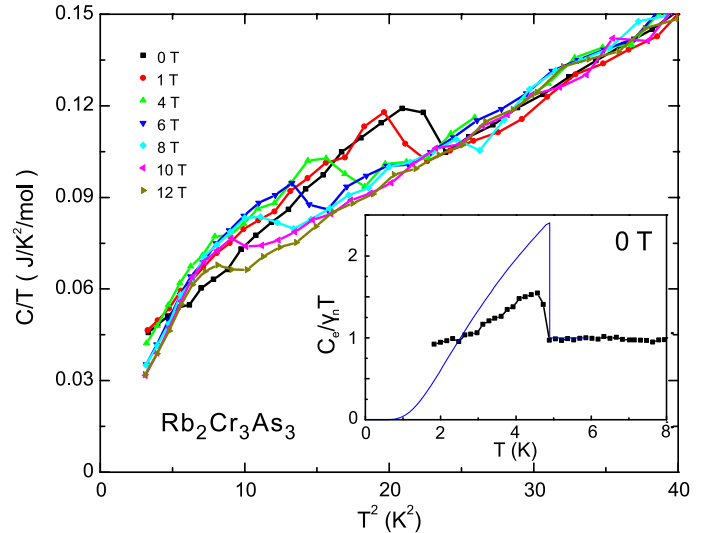


FIG. 5: Heat capacity of  $\text{Rb}_2\text{Cr}_3\text{As}_3$  single crystals with  $H \perp [001]$ . The inset shows the normalized electronic specific heat  $C_e/(\gamma_n T)$  as a function of temperature; blue line is the theoretical BCS expectation for a single-band  $s$ -wave superconductor (see text).

$\text{K}_2\text{Cr}_3\text{As}_3$  and  $\text{Rb}_2\text{Cr}_3\text{As}_3$ , respectively.

Bulk superconductivity in  $\text{Rb}_2\text{Cr}_3\text{As}_3$  is also confirmed by heat capacity measurements on a collection of single crystals (total mass  $\sim 0.2$  mg) oriented with  $H \perp [001]$ , showing a clear jump in specific heat  $C$  at  $T_c$  as shown in Fig. 5. The jump is found to decrease in temperature as magnetic field is increased, indicating the suppression of a bulk superconducting phase transition with field.  $T_c$  obtained from the middle point of the jump were plotted in Fig. 7, which shows remarkably consistency with the transport data. Fitting the normal state heat capacity with the expression  $C/T = \gamma_n + \beta T^2$ , yields values for the electronic Sommerfeld coefficient  $\gamma_n = 39.5 \text{ mJ K}^{-2} \text{ mol}^{-1}$  and the phonon coefficient  $\beta = 2.8 \text{ mJ K}^{-4} \text{ mol}^{-1}$ . The value for  $\gamma_n$  is somewhat smaller than that reported for polycrystalline samples ( $55.1 \text{ mJ K}^{-2} \text{ mol}^{-1}$ ) [2], while that of  $\beta$  is close to previous reports. We extract the electronic component  $C_e$  using these parameters and plot its temperature dependence as  $C_e/(\gamma_n T)$  in the inset of Fig. 5, showing the dimensionless heat capacity jump at  $T_c$  to be  $\Delta C/\gamma_n T_c = 0.62$ , much lower than the reported values of 1.8 in  $\text{Rb}_2\text{Cr}_3\text{As}_3$  [2] and 2.0-2.4 in  $\text{K}_2\text{Cr}_3\text{As}_3$  [1, 10]). It is also lower than the BCS value of 1.43 expected for a conventional superconductor, which could be related to the apparent reduced superconducting volume fraction observed in susceptibility measurements noted above, or more intrinsic origins to do with the nature of superconductivity that require further investigation at lower temperatures.

In order to understand the extent of influence of quasi-1D band structure components on the superconducting state, the anisotropy of  $H_{c2}$  was investigated in both

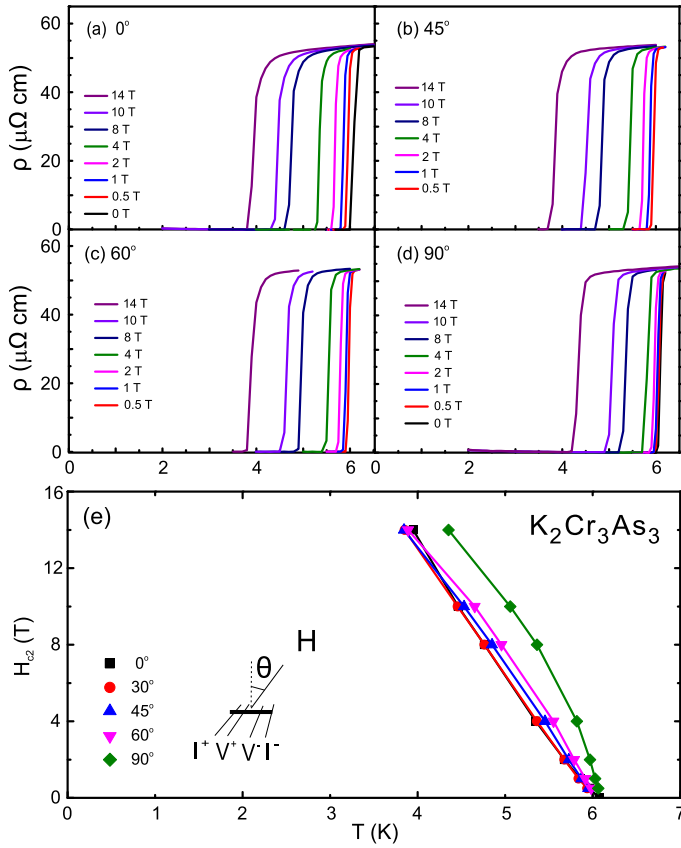


FIG. 6: Upper critical field of  $\text{K}_2\text{Cr}_3\text{As}_3$  single crystal under different field configurations. Panels (a), (b), (c) and (d) present the field evolution of temperature-dependent resistivity under different field orientations with  $\theta = 0^\circ$ ,  $45^\circ$ ,  $60^\circ$  and  $90^\circ$ , respectively. Panel (e) shows the upper critical field temperature dependence in different field orientations as extracted from resistivity transitions in panels (a)-(d), with  $T_c(H)$  defined by the midpoint between zero and full resistance.

$\text{K}_2\text{Cr}_3\text{As}_3$  and  $\text{Rb}_2\text{Cr}_3\text{As}_3$ . The resistive transition was tracked as a function of field angle, as shown in Figs. 6 and 7, using orientation angles  $\theta = 0^\circ$ ,  $45^\circ$ ,  $60^\circ$  and  $90^\circ$  from the  $H_\perp$  orientation for  $\text{K}_2\text{Cr}_3\text{As}_3$  and  $\theta = 0^\circ$  and  $90^\circ$  for  $\text{Rb}_2\text{Cr}_3\text{As}_3$ . For  $\text{K}_2\text{Cr}_3\text{As}_3$ , the initial slope  $dH_{c2}(T_c)/dT$  varies from 5.0 T/K to 16.1 T/K, as observed previously [10], with a rapid increase that is even more significant than what were observed in other quasi-1D superconducting state, as shown in Fig. 8. For  $\text{Rb}_2\text{Cr}_3\text{As}_3$ , the initial slope  $dH_{c2}(T_c)/dT$  has a similar range between  $H_\perp$  and  $H_\parallel$  orientations, with values of 4.4 T/K and 14 T/K, respectively. However, the temperature dependence of  $H_{c2}(T)$  in  $\text{Rb}_2\text{Cr}_3\text{As}_3$  is quite different than that of  $\text{K}_2\text{Cr}_3\text{As}_3$  in the field range up to 14 T, showing a positive curvature for  $H_\perp$  and negative curvature for  $H_\parallel$  as shown in Fig. 7. In fact, the  $H_{c2}(T)$  curves for the two field orientations cross near  $\sim 12$  T, in a manner similar to that observed in other classic quasi-1D superconductors such as  $(\text{TMTSF})_2\text{ClO}_4$  [15]

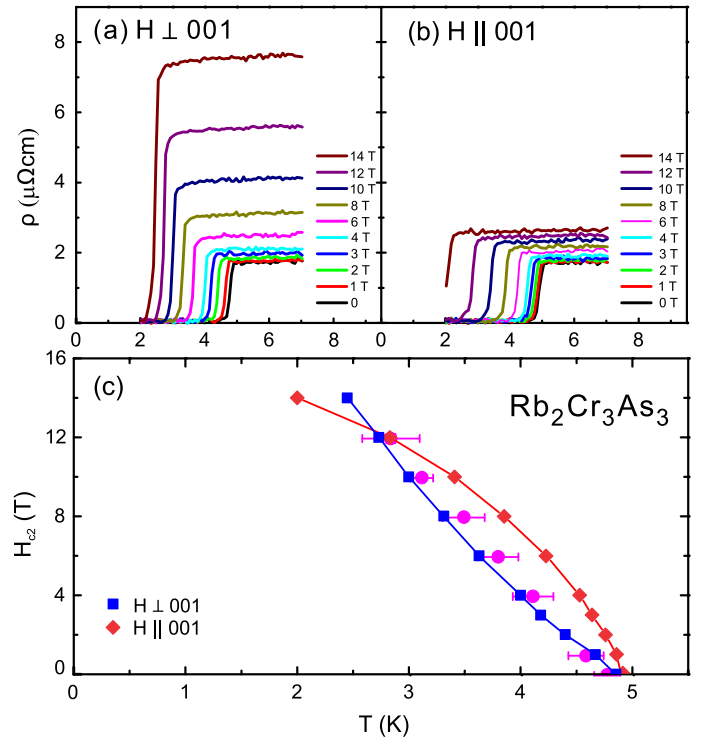


FIG. 7: Upper critical field of  $\text{Rb}_2\text{Cr}_3\text{As}_3$  single crystal under perpendicular (panel (a)) and parallel (panel (b)) field orientations. Temperature dependence of  $H_{c2}$  from resistance data is shown in panel (c), with  $T_c(H)$  defined by the midpoint between zero and full resistance. This is compared with  $T_c(H)$  data obtained from heat capacity with  $H_\perp[001]$  orientation (solid purple circles), with  $T_c$  values defined by the midpoint of the jump in specific heat and error bars corresponding to the transition width.

and  $(\text{TMTSF})_2\text{PF}_6$  [16]. In these organic superconductors, a similar trend is observed where a diverging temperature dependence is observed in the  $H_\perp$  orientation, while a saturating Pauli-limited dependence occurs for  $H_\parallel$  (parallel to the conducting direction). In Li-based purple bronze, such Pauli-limited behavior can be also observed with fields applied along the conducting chain, while a divergent behavior is observed in the other two field orientations [17].

Recent pulsed-field work on  $\text{K}_2\text{Cr}_3\text{As}_3$  single crystals indeed shows such a crossing to occur at higher fields, with  $H_{c2}^\perp(T)$  surpassing  $H_{c2}^\parallel(T)$  near 15 T and indications of Pauli-limited behavior in the  $H_\parallel$  orientation [18]. Fig. 8 presents a comparison between the  $\text{A}_2\text{Cr}_3\text{As}_3$  compounds and the organic systems  $(\text{TMTSF})_2\text{ClO}_4$  and  $(\text{TMTSF})_2\text{PF}_6$ , plotting the temperature dependence of the  $H_{c2}$  anisotropy parameter  $\Gamma(T) = H_{c2}^\parallel(T)/H_{c2}^\perp(T)$  (with  $H_\parallel$  and  $H_\perp$  relative to the  $c$ -axis for  $\text{A}_2\text{Cr}_3\text{As}_3$ , and in the directions of  $a$ - and  $c$ -axis directions, respectively, for TMTSF salts). A similar change in  $\Gamma$ , from large near  $T_c$  to near unity at lower temperatures, is seen in both the organics and  $\text{A}_2\text{Cr}_3\text{As}_3$  materials, in-

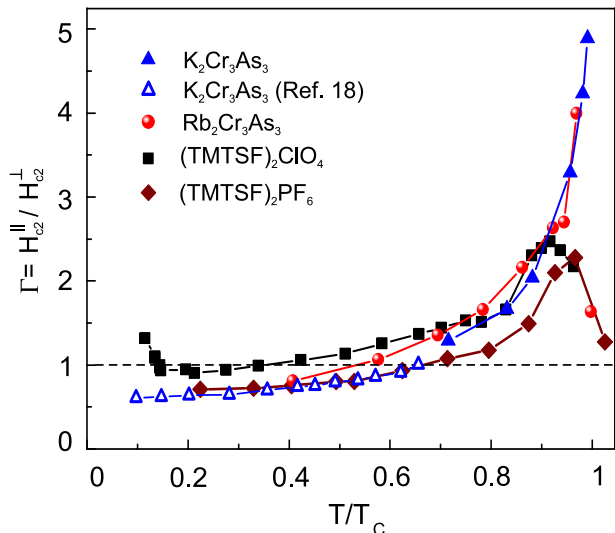


FIG. 8: Anisotropy of the upper critical field  $\Gamma \equiv H_{c2}^{\parallel}(H\parallel 00l \text{ for } 233, H\parallel a \text{ for TMTSF salts})/H_{c2}^{\perp}(H\perp 00l \text{ for } 233, H\parallel b \text{ for TMTSF salts})$ .  $T_c$  of  $K_2Cr_3As_3$  and  $Rb_2Cr_3As_3$  are defined using the midpoint between zero and full resistance. The data for TMTSF salt is taken from Refs. [15] and [16], and high-field data for  $K_2Cr_3As_3$  is from Ref. [18].

indicating a resemblance. Although a similar  $\Gamma(T)$  evolution was also found in higher-dimensional systems such as K-doped  $BaFe_2As_2$  [19, 20], the notable difference is in the crossing (*i.e.*,  $\Gamma=1$ ) point, where the  $H_{\perp}$  component begins to take off in the quasi-1D systems. While a mild anisotropy was previously reported for  $K_2Cr_3As_3$  single crystals [10], it is clear that the observable trend in the limited field range available for our measurements of  $K_2Cr_3As_3$  is very similar to that of  $Rb_2Cr_3As_3$ , and indeed follows the same behavior at higher fields [18] as shown in Fig. 8 for a normalized temperature regime.

Although higher field data for  $Rb_2Cr_3As_3$  is lacking, the apparent likeness of  $\Gamma(T)$  between  $Rb_2Cr_3As_3$  and  $K_2Cr_3As_3$  presents an apparent contradiction: contrasting MR anisotropies are suggestive of a highly tunable quasi-1D normal state electronic structure that differs in the two compounds, while the normalized  $\Gamma(T)$  behavior are very comparable for each. This conundrum could be readily dismissed if Pauli limiting were the dominant pairbreaking mechanism, as the comparison of superconducting condensation energy and Zeeman energy is, to first order, independent of details of the electronic band structure of the host material. However, the observed combination of orbital ( $H_{\perp}$ ) and Pauli ( $H_{\parallel}$ ) limited  $H_{c2}$  behaviors in  $K_2Cr_3As_3$  [18] calls for a less simplified explanation. For instance, the spin-locked Cooper pairing scenario proposed by Balakirev *et al.*, where the pair singlet spins are pinned along the quasi-1D chain direction [18], may provide a pairbreaking scenario common to all  $A_2Cr_3As_3$  superconductors, given their pairing attraction is indeed tied to a low-dimensional spin fluctuation mech-

anism in all three systems. Above all, this highlights the need for detailed experimental studies of the electronic structure as well as higher-field  $H_{c2}$  studies of  $Rb_2Cr_3As_3$  in order to understand how the anisotropy of superconducting state properties is affected by the strongly enhanced normal state anisotropy found in  $Rb_2Cr_3As_3$ .

In summary, we report successful synthesis of high-quality  $A_2Cr_3As_3$  single crystals with  $A = K$  and  $Rb$  using a self-flux method, providing the first comparison of single-crystal properties between two members of this new superconductor family. The increase in ionic size from  $K$  to  $Rb$  causes an increase in the spacing between quasi-one-dimensional chains in the hexagonal crystal structure of  $Rb_2Cr_3As_3$  as compared to  $K_2Cr_3As_3$ , while keeping the intra-chain dimensions mostly unchanged. While the superconducting state properties are comparable between the two systems, the normal state resistivity shows a striking evolution, with a 325% enhancement of magnetoresistance and appearance of strong anisotropy in  $Rb_2Cr_3As_3$ . These properties point to a strong quasi-one-dimensional component in the electronic properties that evolves with enhanced unit cell dimensions in the  $A_2Cr_3As_3$  system. The similarities to other well-established quasi-1D superconductors deserves further attention.

The authors acknowledge R. L. Greene, H. Hodovanets, J. P. Hu, Y. P. Jiang, L. M. Wang, and X. H. Zhang for valuable discussion and experimental assistance. This work was supported by AFOSR through Grant FA9550-14-1-0332 and the Gordon and Betty Moore Foundation's EPiQS Initiative through Grant GBMF4419.

- 
- [1] J. K. Bao, J. Y. Liu, C. W. Ma, Z. H. Meng, Z. T. Tang, Y. L. Sun, H. F. Zhai, H. 8 Jiang, H. Bai, C. M. Feng, Z. A. Xu, and G. H. Cao, Phys. Rev. X 5, 011013 (2015).
  - [2] Z. T. Tang, J. K. Bao, Y. Liu, Y. L. Sun, A. Ablimit, H. F. Zhai, H. Jiang, C. M. Feng, Z. A. Xu, and G. H. Cao, Phys. Rev. B 91, 020506(R) (2015).
  - [3] Z. T. Tang, J. K. Bao, Z. Wang, H. Bai, H. Jiang, Y. Liu, H. F. Zhai, C. M. Feng, Z. A. Xu, and G. H. Cao, Science China Materials 58, 16 (2015).
  - [4] J. Shinagawa, Y. Kurosaki, F. Zhang, C. Parker, S. E. Brown, D. Jerome, J. B. Christensen, and K. Bechgaard Phys. Rev. Lett. 98, 147002(2007)
  - [5] J. Lee, M. J. Naughton, G. M. Danner, and P. M. Chaikin Phys. Rev. Lett. 78, 3555(1997)
  - [6] D. Jerome, A. Mazaud, M. Ribault, K. Bechgaard. Journal de Physique Lettres, 41(4), 95-98(1980).
  - [7] Klaus Bechgaard, Kim Carneiro, Malte Olsen, Finn Berg Rasmussen, and Claus S. Jacobsen. Phys. Rev. Lett. 46, 852(1981)
  - [8] M. Greenblatt, W. H. McCarroll, R. Neifeld, M. Croft, J. V. Waszczak, Solid State Commun. 51, 671 (1984).
  - [9] J. C. Armici, M. Decroux, O. Fischer, M. Potel, R. Chevrel, and M. Sergent, Solid State Commun. 33, 607

- (1980).
- [10] T. Kong, S. L. Bud'ko, and P. C. Canfield, *Phys. Rev. B* 91, 020507(R)(2015).
  - [11] G. M. Pang, M. Smidman, W. B. Jiang, J. K. Bao, Z. F. Weng, Y. F. Wang, L. Jiao, J. L. Zhang, G. H. Cao, and H. Q. Yuan, arXiv:1501.01880v2.
  - [12] H. Z. Zhi, T. Imai, F. L. Ning, J. K. Bao, and G. H. Cao, *Phys. Rev. Lett.* 114, 147004(2015).
  - [13] Kunihiro Kihou et al., *J. Phys. Soc. Jpn.* 79, 124713 (2010).
  - [14] X. X. Wu, C. C. Le, J. Yuan, H. Fan, and J. P. Hu, *Chinese Phys. Lett.* 32 057401(2015).
  - [15] Shingo Yonezawa, S. Kusaba, Y. Maeno, P. Auban-Senzier, C. Pasquier, K. Bechgaard, and D. Jeome, *Phys. Rev. Lett.* 100, 117002(2008).
  - [16] I. J. Lee, M. J. Naughton, G. M. Danner, and P. M. Chaikin, *Phys. Rev. Lett.* 78, 3555(1997).
  - [17] J.-F. Mercure, A. F. Bangura, Xiaofeng Xu, N. Wakeham, A. Carrington, P. Walmsley, M. Greenblatt, and N. E. Hussey *Phys. Rev. Lett.* 108, 187003(2012).
  - [18] F. F. Balakirev, T. Kong, M. Jaime, R. D. McDonald, C. H. Mielke, A. Gurevich, P. C. Canfield, and S. L. Bud'ko, arXiv:1505.05547.
  - [19] M. M. Altarawneh, K. Collar, C. H. Mielke, N. Ni, S. L. Budko, and P. C. Canfield, *Phys. Rev. B* 78, 220505 (2008).
  - [20] H. Q. Yuan, J. Singleton, F. F. Balakirev, S. A. Baily, G. F. Chen, J. L. Luo, and N. L. Wang, *Nature (London)* 457, 565 (2009).